

Southern Ocean dust–climate coupling over the past four million years

Alfredo Martínez-García^{1,2,3}, Antoni Rosell-Melé^{3,4,5}, Samuel L. Jaccard¹, Walter Geibert^{6,7}, Daniel M. Sigman⁸ & Gerald H. Haug^{1,2}

Dust has the potential to modify global climate by influencing the radiative balance of the atmosphere and by supplying iron and other essential limiting micronutrients to the ocean^{1,2}. Indeed, dust supply to the Southern Ocean increases during ice ages, and ‘iron fertilization’ of the subantarctic zone may have contributed up to 40 parts per million by volume (p.p.m.v.) of the decrease (80–100 p.p.m.v.) in atmospheric carbon dioxide observed during late Pleistocene glacial cycles^{3–7}. So far, however, the magnitude of Southern Ocean dust deposition in earlier times and its role in the development and evolution of Pleistocene glacial cycles have remained unclear. Here we report a high-resolution record of dust and iron supply to the Southern Ocean over the past four million years, derived from the analysis of marine sediments from ODP Site 1090, located in the Atlantic sector of the subantarctic zone. The close correspondence of our dust and iron deposition records with Antarctic ice core reconstructions of dust flux covering the past 800,000 years (refs 8, 9) indicates that both of these archives record large-scale deposition changes that should apply to most of the Southern Ocean, validating previous interpretations of the ice core data. The extension of the record beyond the interval covered by the Antarctic ice cores reveals that, in contrast to the relatively gradual intensification of glacial cycles over the past three million years, Southern Ocean dust and iron flux rose sharply at the Mid-Pleistocene climatic transition around 1.25 million years ago. This finding complements previous observations over late Pleistocene glacial cycles^{5,8,9}, providing new evidence of a tight connection between high dust input to the Southern Ocean and the emergence of the deep glaciations that characterize the past one million years of Earth history.

The scarcity of iron reduces marine export production and carbon uptake in one-quarter of the world ocean where the concentration of major nutrients (phosphorus and nitrogen) is perennially high¹⁰ (Fig. 1). The Southern Ocean is the region where variations in iron availability can have the largest effect on Earth’s carbon cycle through its fertilizing effect on marine ecosystems.

In the modern Southern Ocean, deep ocean waters with high CO₂ and nutrient content are brought to the surface by wind-driven upwelling and density-driven overturning. However, the scarcity of iron reduces phytoplankton growth^{1,10}, and major nutrients are returned to the subsurface before they are fully consumed. This incomplete utilization of nutrients represents an important leak in the modern global biological pump because it allows the escape of deeply sequestered carbon back to the atmosphere, thereby raising atmospheric CO₂ levels⁶. Today, the Antarctic zone is the greater part of the Southern Ocean CO₂ leak, because of its extremely low degree of surface nutrient consumption and its ventilation of the abyssal ocean. The subantarctic zone, further north in the Southern Ocean, is characterized by greater nutrient consumption and ventilates the somewhat smaller volume of the mid-depth ocean. However, its nutrient status affects the productivity of the low

latitude ocean, with repercussions for low-latitude CaCO₃ production and for the partitioning of regenerated carbon storage between the mid-depth and deep ocean. Thus, both the Antarctic zone and the subantarctic zone are potentially important for glacial/interglacial CO₂ change^{6,7}.

We first focus on the Antarctic zone. An increase in the efficiency of the global biological pump can be accomplished either by decreasing the physical cycling of deep water through the surface of the Antarctic zone¹¹ or by increasing the degree to which Antarctic zone surface nutrients are consumed by marine organisms (for example, as a result of an increase in the availability of iron relative to other nutrients^{6,12}). Data and models have been used to argue that the Antarctic was more strongly stratified during ice ages, reducing the Antarctic leak in the biological pump^{6,12}. Because Antarctic major nutrient and iron supply come from upwelled water, productivity in the Antarctic zone would probably decline during ice ages in step with stratification, consistent with most Antarctic productivity data⁴. Nevertheless, the greater the input of aeolian iron, the greater the degree of nutrient consumption is expected for a given increase in Antarctic stratification, because the dust input raises the total iron supply to the surface ocean relative to the input of major nutrients and excess CO₂ from below^{6,7}. Thus, dust input to the Antarctic is a central regulator of how completely the Antarctic CO₂ leak can be sealed during ice ages, regardless of whether productivity increased or decreased in the region.

Second, we consider the subantarctic zone. This zone, unlike the Antarctic, is characterized by higher productivity during ice ages^{4,5,13}.

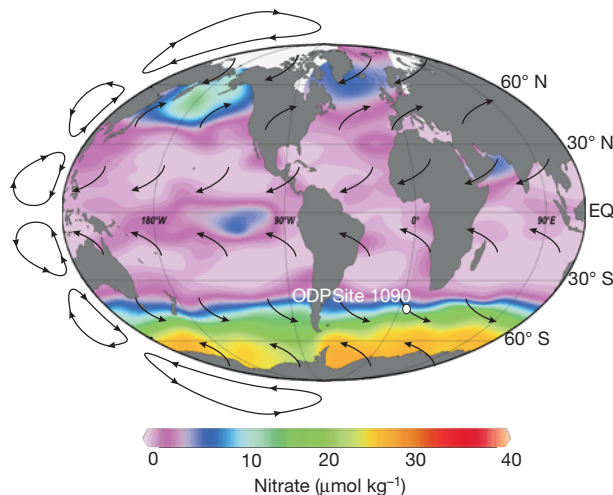


Figure 1 | Location of ODP Site 1090, world ocean surface nitrate concentrations, and wind direction. ODP Site 1090, the source of the sediment cores used in this study, is located at 42° 54.5' S, 8° 54.0' E, at 3,702 m depth. Nitrate concentrations are from the Electronic Atlas of the World Ocean Experiment. Black arrows are schematic representations of atmospheric convection cells and wind directions. EQ, Equator.

¹Geological Institute, ETH Zürich, Zürich 8092, Switzerland. ²DFG-Leibniz Center for Surface Process and Climate Studies, Institute for Geosciences, Potsdam University, Potsdam D-14476, Germany. ³Institut de Ciència i Tecnologia Ambientals (ICTA), Universitat Autònoma de Barcelona, Bellaterra 08193, Catalonia, Spain. ⁴Institució Catalana de Recerca i Estudis Avançats (ICREA), Barcelona 08010, Catalonia, Spain. ⁵College of Oceanic and Atmospheric Sciences, Oregon State University, Corvallis, Oregon 97331-5503, USA. ⁶School of GeoSciences, The University of Edinburgh, Edinburgh EH9 3JW, UK. ⁷Scottish Association for Marine Science (SAMS), Scottish Marine Laboratory, Oban, Argyll PA37 1QA, UK. ⁸Department of Geosciences, Princeton University, New Jersey 08544, USA.

This suggests a conceptually simpler mechanism than in the Antarctic zone by which dust-driven iron fertilization of the subantarctic zone may have lowered atmospheric CO₂, with the increase in subantarctic zone productivity consuming a greater fraction of the surface nutrients and thus driving more storage of carbon in the ocean interior. The subantarctic zone is one of the best candidates for aeolian iron fertilization, because it falls in the same latitude as the major Southern Hemisphere dust sources, and is on the wind path from them^{3,6}. Further, there is evidence that natural aeolian iron deposition enhances marine export production in the modern subantarctic zone¹⁴. Palaeoceanographic data appear to constrain its effect to a maximum of 40 p.p.m.v. of the atmospheric CO₂ decrease observed in the last glacial cycle, because a significant increase in dust fluxes and marine export production in the subantarctic zone is only observed in the transition from marine isotope stage (MIS) 5 to MIS 4, when atmospheric CO₂ concentrations are already around 40–50 p.p.m.v. lower than during the interglacial periods^{3–7}. A CO₂ drawdown of ≤40 p.p.m. from subantarctic zone iron fertilization is consistent with estimates obtained using geochemical box models and Earth system models, which in most cases range between 20 and 40 p.p.m.v. (see refs 3, 7, 15–18 and Supplementary Information).

The ice core reconstruction generated by the EPICA project^{8,9} has provided a unique record with which to test dust–climate interactions in the Southern Ocean over the past 800,000 years (Fig. 2d). However, ice core records only allow an indirect inference of the supply of dust and iron to the ocean, and it is unclear how far back in time they can be extended¹⁹. Here we report a high-resolution dust and iron record from the subantarctic Atlantic spanning the past four million years (4 Myr), which provides the first insights into the variability of Southern Ocean dust deposition through the major climatic transitions of the Pliocene and Pleistocene epochs.

The record is based on the combined analysis of independent organic (*n*-alkanes) and inorganic (Fe, Ti and ²³²Th) dust proxies in

marine sediments from ODP Site 1090 (Fig. 1). Long-chain *n*-alkanes are lipid constituents of the epicuticular wax layer of terrestrial plants. These terrestrial lipids are eroded from leaf surfaces and soils by winds and transported in the organic fraction of aeolian dust over the ocean²⁰. In our record, there is a clear predominance of long-chain *n*-alkanes with odd carbon numbers over those with even carbon numbers, over the Pliocene and Pleistocene epochs. This is representative of inputs of leaf waxes from terrestrial plants transported by wind²⁰, supporting the interpretation of the record in terms of changes in dust deposition through time⁵. Fe, Ti and ²³²Th are elements with a well-characterized lithogenic origin. Hence, their concentration in marine sediments can be used to quantitatively estimate variations in the supply of wind-borne lithogenic material to remote areas of the ocean where other sources of continental material are negligible^{5,13,21} (see Supplementary Information). The consistency among the different dust tracers measured in ODP Site 1090 and their excellent correlation with the dust deposition record from the Antarctic ice cores over the past 0.8 Myr (Fig. 2d) indicate that they are faithful recorders of changes in the supply of dust, and hence of iron, to high southern latitudes through time. This subantarctic zone/ice-core agreement in dust flux history also validates the long-held assumption that the ice core records reflect the pattern of dust fluxes to the Southern Ocean surface. A difference in the magnitude of the glacial–interglacial change of dust flux between ocean sediment and polar ice core records has been noted previously^{5,8}. We note a similar difference here, with our record indicating a smaller glacial–interglacial change compared with the changes of more than an order of magnitude indicated by the Antarctic ice cores (Fig. 2d). This difference is probably due to variations in the efficiency of dust transport mechanisms to the Antarctic continent during glacial stages⁸.

Our record reveals that, on orbital timescales, Southern Ocean dust deposition has been exponentially linked to global ice volume changes through the Pliocene and Pleistocene epochs (Fig. 2). Major steps in

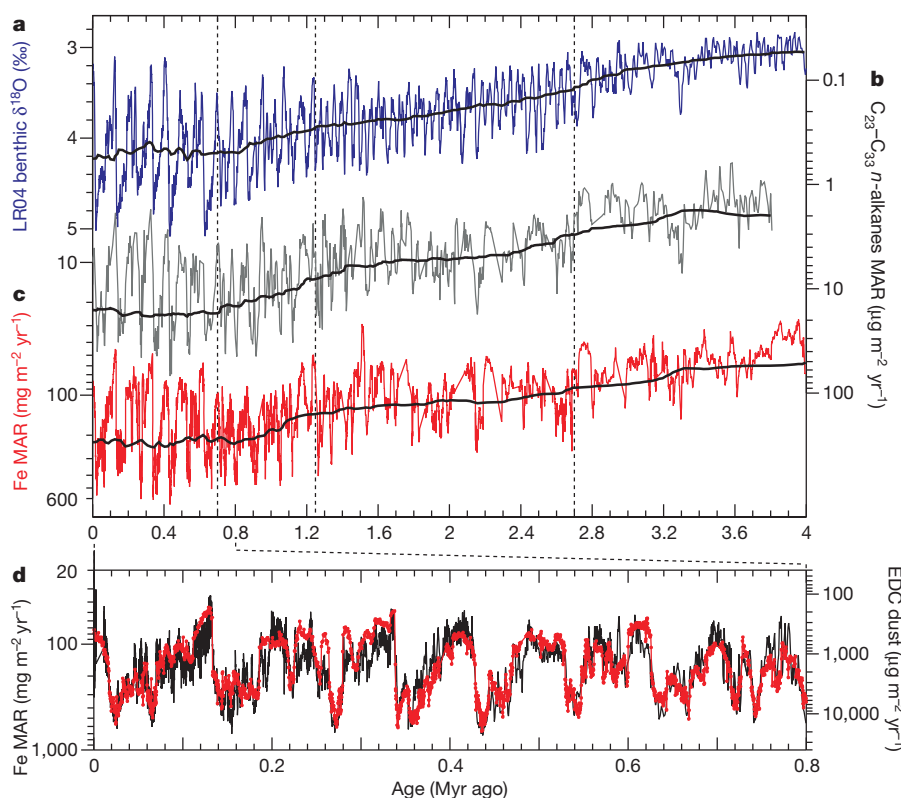


Figure 2 | Global ice volume, dust and iron deposition in the Southern Ocean since 4 Myr ago. **a**, Lisiecki and Raymo (LR04) benthic $\delta^{18}\text{O}$ stack²⁸. **b**, **c**, Mass accumulation rates (MARs) of *n*-alkanes (**b**) and iron (**c**) at ODP Site 1090. Both records are plotted on a reversed logarithmic scale to emphasize the

exponential relationship with the benthic $\delta^{18}\text{O}$ record. **d**, Expanded view of iron variability over the past 800 kyr at ODP Site 1090 (red line), plotted together with dust flux estimates in the Antarctic ice core from EPICA Dome C (EDC; black line)⁸.

dust deposition coincide with the two major climatic transitions of the Pliocene–Pleistocene, indicating a pervasive link between Southern Ocean dust and Northern Hemisphere glaciations.

The first significant rise in ice-age dust and iron deposition is observed around 2.7 Myr ago, coinciding with the initiation of major glaciations in the Northern Hemisphere (Figs 1 and 2). The development of large, perennial Northern Hemisphere ice sheets around 2.7 Myr ago represents a milestone in climate evolution that marks the end of the relatively stable Pliocene warm period and the emergence of strong feedbacks in the climate system that characterize Quaternary climate oscillations. Although Earth's orbital configuration favoured the initiation of regional glaciations, a decrease in atmospheric CO₂ concentrations may be required to initiate and sustain larger glaciations²². Data from the Antarctic zone and the subarctic North Pacific suggest that a transition towards permanent polar ocean water-column stratification identified around 2.7 Myr ago may have been a key driver of this CO₂ decline²³. Our data indicate that Antarctic zone stratification may have been reinforced by an increase in iron supply to the Southern Ocean during glacial stages after 2.7 Myr ago, and a similar dynamic may have applied to the subarctic North Pacific.

During the Pliocene, meridional temperature gradients were relatively weak, and the tropical warm pool was apparently more expansive than today^{24,25}. This climate state resulted in relatively weak atmospheric convective cells that extended further poleward, greatly affecting wind intensity and global precipitation patterns²⁴. As a result of these conditions, models predict stronger precipitation over Africa, Australia and South America during Pliocene times²⁴, which, together with a weak atmospheric circulation, would have minimized dust generation and transport in these regions. Thus, the strengthening of the meridional temperature gradients at the 2.7-Myr transition and the mid-Pleistocene transition (MPT) as a consequence of the increase in ice volume would have resulted in intensification and spatial contraction of the atmospheric convective cells^{24,25} and a reduction in precipitation; these effects would have favoured dust generation and transport, consistent with the increases in dust and iron flux observed at Site 1090.

The most dramatic rise in dust deposition in our record occurs across the MPT (Fig. 3). During this period, Southern Ocean dust fluxes doubled, reaching peak fluxes comparable to those of the Last Glacial Maximum. Although the controls on Southern Ocean dust deposition are not well understood, previous studies have suggested that dust generation requires that a climate threshold must be reached before the system is sensitive to perturbation^{5,8,18}. Taking the last glacial cycle as an example, dust flux changed relatively little during the initial climate deterioration during MIS 5, increasing abruptly at MIS 4 with the rapid increase in Northern Hemisphere ice^{5,7}. Our long-term dust flux and iron deposition records are strongly convergent with this view, and reveal that Southern Ocean dust flux has a unique sensitivity to the very cold glacial conditions that characterize the past 1.25 Myr. Whereas measures of climate cooling and glaciation indicate a relatively gradual trend in mean climate over the Pleistocene, dust flux at Site 1090 increases exponentially at the MPT, when the most intense ice ages first appear (Fig. 3). The data thus confirm and extend the evidence for a nonlinear relationship of Southern Ocean dust flux to climate (Fig. 3b), indicating that it applies to the entire Pliocene–Pleistocene. This sensitivity of dust flux to climate is also consistent with the observations of relatively constant interglacial tropical sea surface temperature and atmospheric CO₂ across the MPT^{26,27}, as no significant changes in interglacial dust deposition are observed.

Beginning at 1.25 Myr ago, the MPT was characterized by the development of thicker and less stable ice-sheets in the Northern Hemisphere and the emergence of the high-amplitude, asymmetric 100-kyr cycle that distinguishes late Pleistocene glaciations^{28,29}. This important climatic shift occurred in the absence of any significant change in orbital forcing, leading to the view that the MPT involved a reorganization of the climate system's internal feedbacks²⁹. A

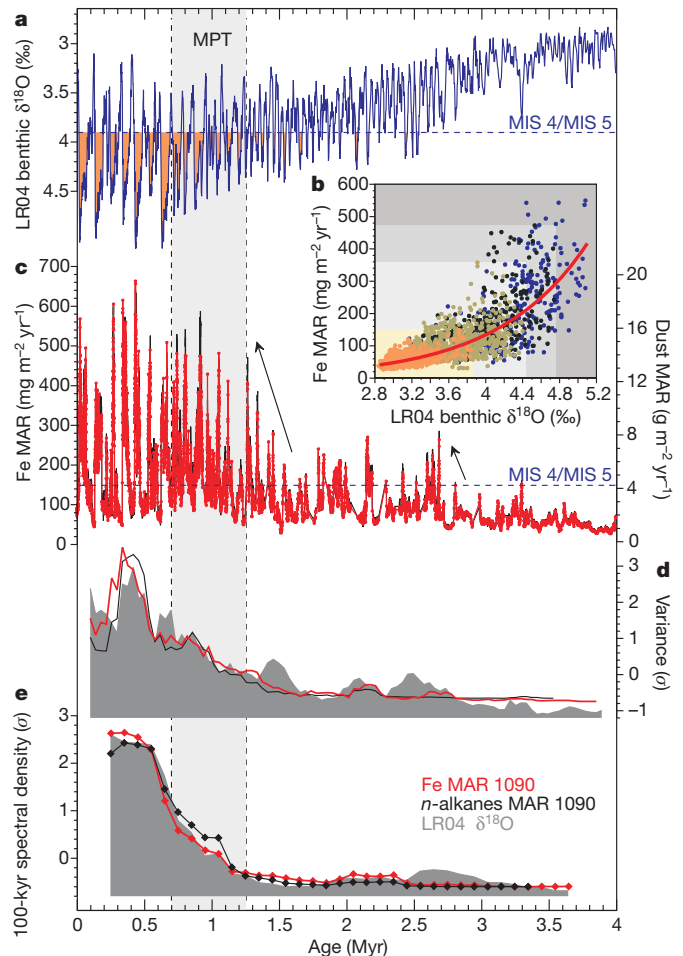


Figure 3 | Evolution of global ice volume, and Southern Ocean dust and iron variability through the Pliocene and Pleistocene epochs. **a**, Benthic $\delta^{18}\text{O}$ stack²⁸. Orange shading indicates the intervals where glaciations intensified and dust fluxes rose to levels comparable to those of the Marine Isotope Stage (MIS) 5 to MIS 4 transition. **b**, Regression between benthic $\delta^{18}\text{O}$ and Fe MAR. Colours indicate key time intervals: 0–0.7 Myr ago (blue), 0.7–1.25 Myr ago (black), 1.25–2.7 Myr ago (brown) and 2.7–4 Myr ago (orange). Background shading areas highlight the evolution of the Fe MAR/benthic $\delta^{18}\text{O}$ coupling across the defined key time intervals. **c**, Fe MAR (red line), and dust MAR estimated from the Ti MAR (black line). **d**, Normalized variance of Fe MAR, *n*-alkanes MAR, and benthic $\delta^{18}\text{O}$, computed in 200-kyr windows with a number of lags equal to half the timeseries length (' $\frac{1}{2}$ lags'); key given in **e**. **e**, Normalized power spectral density of the 100-kyr cycle in Fe MAR, *n*-alkanes MAR and $\delta^{18}\text{O}$ computed using 500-kyr windows and $\frac{1}{2}$ lags. Vertical dashed lines with grey shading between indicate start and finish of MPT according to ref. 29. In **d** and **e**, the variance and the power spectral density of the 100-kyr cycle of the different records were normalized to zero mean and unit standard deviation (σ).

decrease in atmospheric CO₂ concentrations and the associated global cooling is often proposed as one of the mechanisms to explain the MPT²⁹. The available data do indeed suggest that atmospheric CO₂ concentrations during peak ice age conditions decreased by ~ 30 p.p.m. across the MPT²⁶.

Although our data cannot yet enable us to prove causation, they raise the strong possibility that dust not only increased into the stronger ice ages of the post-MPT world but then also acted as a positive feedback, encouraging further CO₂ reduction and cooling through iron fertilization of the Southern Ocean. Consistent with this hypothesis, an increase in opal mass accumulation rate (MAR) has also been observed in the Atlantic sector of the Southern Ocean during this period, coinciding with the development of extensive diatom mats between 47° S and 50° S and with the emergence of the diatom *Fragilariopsis kerguelensis*, the dominant species in modern Southern Ocean sediments³⁰. These

observations suggest that an increase in iron availability may have driven part or all of the 30 p.p.m.v. decrease in peak glacial atmospheric CO₂ observed across the MPT. By driving the descent into deep, cold glacial periods, the climate/dust/CO₂ feedback may underpin the development of the strong 100-kyr periodicity that characterizes global climate and dust since the MPT (Fig. 3e). In detail, the greater ice-age dust loads may have increased carbon sequestration by both the Antarctic zone—where it would have encouraged increasingly complete major nutrient consumption even if circulation changes lowered total ice age productivity—and the subantarctic zone, where ice age iron fertilization appears to have fuelled a simple increase in export production.

METHODS SUMMARY

The methods used in the analysis of *n*-alkanes, Fe, Ti and ²³²Th have been described in detail elsewhere⁵. The high-resolution records of Fe and Ti measured with the X-ray fluorescence (XRF) core-scanner were converted into quantitative concentrations using more than 400 inductively coupled plasma sector-field mass spectrometry (ICP-SFMS) measurements (Supplementary Fig. 1). Dry bulk density (DBD) was estimated for each XRF measurement interval from the γ -ray attenuation (GRA) density measurements performed in the same sediment sections as the XRF. MAR was calculated by multiplying the concentration of the different compounds by the DBD and the sedimentation rate. After error propagation, we find that the analytical component of the uncertainty is 7.8%, 8.4% and 8.6% of the final value (1σ) for Fe, Ti and *n*-alkanes MAR, respectively. The influence of age model uncertainty on the estimated MAR is evaluated in Supplementary Fig. 6. Our results show that the analytical uncertainty and the potential errors in the age model do not result in significant deviations from the estimated MAR that would affect the conclusions of this study.

Full Methods and any associated references are available in the online version of the paper at www.nature.com/nature.

Received 14 February; accepted 16 June 2011.

Published online 3 August 2011.

- Martin, J. H., Gordon, R. M. & Fitzwater, S. E. Iron in Antarctic waters. *Nature* **345**, 156–158 (1990).
- Martin, J. Glacial-interglacial CO₂ change: the iron hypothesis. *Paleoceanography* **5**, 1–13 (1990).
- Watson, A. J., Bakker, D. C. E., Ridgwell, A. J., Boyd, P. W. & Law, C. S. Effect of iron supply on Southern Ocean CO₂ uptake and implications for glacial atmospheric CO₂. *Nature* **407**, 730–733 (2000).
- Kohfeld, K. E., Le Quere, C., Harrison, S. P. & Anderson, R. F. Role of marine biology in glacial-interglacial CO₂ cycles. *Science* **308**, 74–78 (2005).
- Martinez-Garcia, A. *et al.* Links between iron supply, marine productivity, sea surface temperature, and CO₂ over the last 1.1 Ma. *Paleoceanography* **24**, PA1207, doi:10.1029/2008PA001657 (2009).
- Sigman, D. M., Hain, M. P. & Haug, G. H. The polar ocean and glacial cycles in atmospheric CO₂ concentration. *Nature* **466**, 47–55 (2010).
- Hain, M. P., Sigman, D. M. & Haug, G. H. Carbon dioxide effects of Antarctic stratification, North Atlantic Intermediate Water formation, and subantarctic nutrient drawdown during the last ice age: diagnosis and synthesis in a geochemical box model. *Glob. Biogeochem. Cycles* **24**, GB4023, doi:10.1029/2010gb003790 (2010).
- Lambert, F. *et al.* Dust-climate couplings over the past 800,000 years from the EPICA Dome C ice core. *Nature* **452**, 616–619 (2008).
- Wolff, E. W. *et al.* Southern Ocean sea-ice extent, productivity and iron flux over the past eight glacial cycles. *Nature* **440**, 491–496 (2006).
- Boyd, P. W. *et al.* Mesoscale iron enrichment experiments 1993–2005: synthesis and future directions. *Science* **315**, 612–617 (2007).
- Toggweiler, J. R. Variation of atmospheric CO₂ by ventilation of the ocean's deepest water. *Paleoceanography* **14**, 571–588 (1999).
- François, R. *et al.* Contribution of Southern Ocean surface-water stratification to low atmospheric CO₂ concentrations during the last glacial period. *Nature* **389**, 929–935 (1997).
- Kumar, N. *et al.* Increased biological productivity and export production in the glacial Southern Ocean. *Nature* **378**, 675–680 (1995).
- Cassar, N. *et al.* The Southern Ocean biological response to aeolian iron deposition. *Science* **317**, 1067–1070 (2007).
- Matsumoto, K., Sarmiento, J. L. & Brzezinski, M. A. Silicic acid leakage from the Southern Ocean: a possible explanation for glacial atmospheric pCO₂. *Glob. Biogeochem. Cycles* **16**, 1031, doi:10.1029/2001GB001442 (2002).
- Brovkin, V., Ganopolski, A., Archer, D. & Rahmstorf, S. Lowering of glacial atmospheric CO₂ in response to changes in oceanic circulation and marine biogeochemistry. *Paleoceanography* **22**, PA4202, doi:10.1029/2006PA001380 (2007).
- Kohler, P., Fischer, H., Munhoven, G. & Zeebe, R. E. Quantitative interpretation of atmospheric carbon records over the last glacial termination. *Global Biogeochem. Cycles* **19**, GB4020, doi:10.1029/2004GB002345 (2005).
- Ridgwell, A. J. Implications of the glacial CO₂ “iron hypothesis” for Quaternary climate change. *Geochem. Geophys. Geosyst.* **4**, 1076, doi:10.1029/2003GC000563 (2003).
- Jouzel, J. & Masson-Delmotte, V. Deep ice cores: the need for going back in time. *Quat. Sci. Rev.* **29**, 3683–3689 (2010).
- Simoneit, B. R. T., Chester, R. & Eglinton, G. Biogenic lipids in particulates from the lower atmosphere over the eastern Atlantic. *Nature* **267**, 682–685 (1977).
- Winckler, G., Anderson, R. F., Fleisher, M. Q., McGee, D. & Mahowald, N. Covariant glacial-interglacial dust fluxes in the equatorial Pacific and Antarctica. *Science* **320**, 93–96 (2008).
- Lunt, D. J., Foster, G. L., Haywood, A. M. & Stone, E. J. Late Pliocene Greenland glaciation controlled by a decline in atmospheric CO₂ levels. *Nature* **454**, 1101–1105 (2008).
- Sigman, D. M., Jaccard, S. L. & Haug, G. H. Polar ocean stratification in a cold climate. *Nature* **428**, 59–63 (2004).
- Brierley, C. M. *et al.* Greatly expanded tropical warm pool and weakened Hadley Circulation in the early Pliocene. *Science* **323**, 1714–1718 (2009).
- Martinez-Garcia, A., Rosell-Mele, A., McClymont, E. L., Gersonde, R. & Haug, G. H. Subpolar link to the emergence of the modern equatorial Pacific Cold Tongue. *Science* **328**, 1550–1553 (2010).
- Honisch, B., Hemming, N. G., Archer, D., Siddall, M. & McManus, J. F. Atmospheric carbon dioxide concentration across the mid-Pleistocene transition. *Science* **324**, 1551–1554 (2009).
- Herbert, T. D., Peterson, L. C., Lawrence, K. T. & Liu, Z. Tropical ocean temperatures over the past 3.5 million years. *Science* **328**, 1530–1534 (2010).
- Lisiecki, L. E. & Raymo, M. E. A Pliocene-Pleistocene stack of 57 globally distributed benthic $\delta^{18}\text{O}$ records. *Paleoceanography* **20**, PA1003, doi:10.1029/2004PA001071 (2005).
- Clark, P. U. *et al.* The middle Pleistocene transition: characteristics, mechanisms, and implications for long-term changes in atmospheric pCO₂. *Quat. Sci. Rev.* **25**, 3150–3184 (2006).
- Cortese, G. & Gersonde, R. Plio/Pleistocene changes in the main biogenic silica carrier in the Southern Ocean, Atlantic Sector. *Mar. Geol.* **252**, 100–110 (2008).

Supplementary Information is linked to the online version of the paper at www.nature.com/nature.

Acknowledgements We thank S. Stefer for performing the XRF scanner measurements at the University of Bremen; and I. Vöge for assistance in the ICP-SFMS analysis at the Alfred Wegener Institute for Polar and Marine Research. We thank the Integrated Ocean Drilling Program for providing the samples used in this study. This research used data acquired at the XRF Core Scanner Laboratory at the MARUM – Center for Marine Environmental Sciences, University of Bremen. Support for this work was provided by the Spanish Ministry of Science and Innovation (MICINN), the European Commission, and the Deutsche Forschungsgemeinschaft (DFG).

Author Contributions A.M.-G., A.R.-M. and G.H.H. designed the study. A.M.-G. performed the *n*-alkane and elemental ICP-SFMS analysis and wrote the first version of the manuscript. G.H.H. and S.L.J. organized and supervised the XRF scanning at the University of Bremen. W.G. organized and supervised the ICP-SFMS elemental analysis at the Alfred Wegener Institute. All the authors contributed to the interpretation of the data and provided significant input to the final manuscript.

Author Information Reprints and permissions information is available at www.nature.com/reprints. The authors declare no competing financial interests. Readers are welcome to comment on the online version of this article at www.nature.com/nature. Correspondence and requests for materials should be addressed to A.M.-G. (alfredo.martinez-garcia@erdw.ethz.ch).

METHODS

Analysis of *n*-alkanes. The method used for analysis of *n*-alkanes has been described in detail elsewhere^{5,31,32}. Briefly, sediment samples were freeze-dried, homogenized, microwave extracted, and analysed with a Thermo Trace GC-FID. The identification of the different compounds was achieved through comparison of the chromatographic relative retention times with those of the target compounds in standards. Several selected samples were analysed by mass spectrometry to confirm peak identities and the absence of co-eluting peaks. The reproducibility of the procedure was evaluated using a homogeneous sediment standard, extracted with every batch of 14 samples. The external analytical reproducibility in the determination of *n*-alkanes in the different batches analysed was 7%.

ICP-SFMS analysis of Fe, Ti, ²³²Th. The methods used in the analysis of Fe, Ti and ²³²Th have been described in detail elsewhere⁵. Briefly, sediment samples were freeze-dried and digested in a pressure-assisted microwave system using an acid mixture of HNO₃, HCl and HF. Fe, Ti and ²³²Th concentrations were determined by inductively coupled plasma sector-field mass spectrometry (ICP-SFMS, Element2, Thermo Scientific). The calibration was done with dilutions of a standard solution, and Rh was used as internal standard. External reproducibility was evaluated using the NIST standard reference material 2702 ("inorganics in marine sediment"), and with each batch of samples, two procedural blanks were run. The average relative error for Fe and Ti was respectively 1.8% and 2.1% (1 σ), and the external reproducibility of NIST 2702 was 5.6% and 6.5% respectively, for the batches included in Supplementary Fig. 1.

XRF scanner measurements. The high resolution elemental analysis of Fe and Ti was performed using an Aavatech profiling X-ray Fluorescence (XRF) core scanner at Bremen University at a 1 cm downcore resolution. The external reproducibility of the Aavatech XRF core scanner for Fe and Ti in the range of the measurements is below 2% (1 σ).

Age model. In the interval 0–800 kyr ago, we use the age model generated by graphic correlation of the XRF Fe measurements to the ice core dust reconstruction from the EPICA project⁸ (Supplementary Fig. 2). This allows us to compare the marine and continental records on similar timescales. In the interval 800–2,900 kyr ago, we use the original age model of ODP Site 1090 based on benthic $\delta^{18}\text{O}$ stratigraphy³³. In the older part of the record we have slightly modified the age model based on biostratigraphy^{34,35} by aligning the *n*-alkane record to the Lisiecki and Raymo (LR04) global benthic $\delta^{18}\text{O}$ stack (see Supplementary Fig. 3). **Mass accumulation rate (MAR) calculation.** The high-resolution estimates of Fe and Ti measured with the XRF core-scanner have been converted into quantitative

concentrations using more than 400 ICP-SFMS measurements. The correlation coefficients and the regression lines used for the calculation are shown in Supplementary Fig. 1. Dry bulk density (DBD) has been estimated for each XRF measurement interval from the γ -ray attenuation (GRA) density measurements³⁵ performed in the same sediment sections as the XRF. GRA bulk density has been converted into DBD using the regression line shown in Supplementary Fig. 1a, which is obtained from the cross-correlation of the GRA density and the available DBD discrete measurements³⁵. The errors associated with the DBD are less 5% of the estimated value³⁶. MARs were calculated by multiplying the concentration of the different compounds by the DBD and the sedimentation rate.

MAR uncertainty. In order to assess the uncertainty in the MAR of the different elements, we consider the errors of the different measurements and how they are propagated in the calculation. In order to do so, we distinguish between statistical errors, derived from the uncertainty associated with the analysis, and systematic deviations, as potentially present in the age model. Systematic deviations of the age model cannot be treated like statistical errors, as they do not meet the requirements for the underlying mathematics. After error propagation, we find that the analytical component of the uncertainty is 7.8%, 8.4% and 8.6% of the final value (1 σ) for Fe, Ti and *n*-alkanes MAR respectively. The influence of age model uncertainty on the estimated MAR is evaluated in Supplementary Fig. 6. Maximum age model error envelopes of 4 kyr, 6 kyr and 15 kyr for the intervals 0–1 Myr ago, 1–3 Myr ago and 3–4 Myr ago respectively²⁸ do not allow for significant changes in the estimated MAR that would affect the conclusions of this study.

31. McClymont, E. L., Martinez-Garcia, A. & Rosell-Mele, A. Benefits of freeze-drying sediments for the analysis of total chlorins and alkenone concentrations in marine sediments. *Org. Geochem.* **38**, 1002–1007 (2007).
32. Kornilova, O. & Rosell-Mele, A. Application of microwave-assisted extraction to the analysis of biomarker climate proxies in marine sediments. *Org. Geochem.* **34**, 1517–1523 (2003).
33. Venz, K. A. & Hodell, D. A. New evidence for changes in Plio-Pleistocene deep water circulation from Southern Ocean ODP Leg 177 Site 1090. *Palaeogeogr. Palaeoclimatol. Palaeoecol.* **182**, 197–220 (2002).
34. Zielinski, U. & Gersonde, R. Plio-Pleistocene diatom biostratigraphy from ODP Leg 177, Atlantic sector of the Southern Ocean. *Mar. Micropaleontol.* **45**, 225–268 (2002).
35. Gersonde, R. *et al.* Southern Ocean paleoceanography. Sites 1088–1094. *Proc. ODP Init. Rep.* **177**, (1999).
36. Blum, P. *Physical Properties Handbook: A Guide to the Shipboard Measurement of Physical Properties of Deep-Sea Cores* (ODP Tech. Note 26, 1997).